Assisting and opposing mixed convection with conjugate heat transfer in a differentially heated cavity filled with coarse-grained porous media

Chakkingal, Manu; de Geus, Julia; Kenjereš, Saša; Ataei-Dadavi, Iman; Tummers, M. J.; Kleijn, Chris R.

DOI
10.1016/j.icheatmasstransfer.2019.104457

Publication date
2020

Document Version
Final published version

Published in
International Communications in Heat and Mass Transfer

Citation (APA)
Chakkingal, M., de Geus, J., Kenjereš, S., Ataei-Dadavi, I., Tummers, M. J., & Kleijn, C. R. (2020). Assisting and opposing mixed convection with conjugate heat transfer in a differentially heated cavity filled with coarse-grained porous media. *International Communications in Heat and Mass Transfer*, *111*, Article 104457. https://doi.org/10.1016/j.icheatmasstransfer.2019.104457

International Communications in Heat and Mass Transfer 111 (2020) 104457

Contents lists available at ScienceDirect

International Communications in Heat and Mass Transfer

journal homepage: www.elsevier.com/locate/ichmt

Assisting and opposing mixed convection with conjugate heat transfer in a differentially heated cavity filled with coarse-grained porous media

Manu Chakkingal[a,*,1], Julia de Geus[a,1], Saša Kenjereš[a], Iman Ataei-Dadavi[a], M.J. Tummers[b], Chris R. Kleijn[a]

[a] Transport Phenomena Section, Department of Chemical Engineering, Delft University of Technology, Delft, the Netherlands
[b] Fluid Mechanics Section, Department of Process and Energy, Delft University of Technology, Delft, the Netherlands

ARTICLE INFO

Keywords:
Natural convection
Assisting and opposing mixed convection
Porous media
Local temperature and flow distribution
Darcy simulation
Quasi-steady flow
Laminar flow

ABSTRACT

We report numerical simulations of assisting and opposing mixed convection in a side-heated, side-cooled cavity packed with relatively large solid spheres. The mixed convection is generated by imposing a movement on the isothermal vertical walls, either in or opposite to the direction of natural convection flow. For a fluid Prandtl number of 5.4 and fluid Rayleigh numbers of 10^6 and 10^7, we varied the modified Richardson number from 0.025 to 500. As in fluids-only mixed convection, we find that the mutual interaction between forced and natural convection, leading to a relative heat transfer enhancement in assisting - and a relative heat transfer suppression in opposing - mixed convection, is most prominent at a Richardson number of approximately one, when the Richardson number is modified with the Darcy number Da and the Forchheimer coefficient $C_f = 0.1$ as $Ri_m = Ri \times Da^{0.5}/C_f$. We focus on local flow and heat transfer variations in order to explain differences in local and average heat transfer between a coarse grained and fine grained (Darcy-type) porous medium, at equal porosity and permeability. We found that the ratio between the thermal boundary layer thickness at the isothermal walls and the average pore size plays an important role in the effect that the grain and pore size have on the heat transfer. When this ratio is relatively large, the thermal boundary layer is locally disturbed by the solid objects and these objects cause local velocities and flow recirculation perpendicular to the walls, resulting in significant differences in the wall-averaged heat transfer. The local nature of the interactions between flow and solid objects cannot be captured by a volume averaged approach, such as a Darcy model.

1. Introduction

In many real-life applications with forced convective heat transfer, the simultaneous effect of natural convection cannot be neglected. Several reported studies on this so-called mixed convection demonstrated the importance of considering natural convection effects along with imposed forced convection in the laminar [1,2], laminar-turbulent transition and turbulent flow [3] regimes. The heat transfer mechanism of mixed convection differs from that of natural convection and forced convection because of the strong coupling between the externally imposed flow and the flow induced by density gradients as a result of temperature gradients. Thus, in addition to the fluid's Prandtl number (Pr), mixed convection heat transfer is generally governed by two dimensionless numbers, viz. the Rayleigh number (Ra) – which is a measure for the strength of natural convection heat transfer - and the Péclet number (Pe)– which is a measure for the strength of forced convection heat transfer. The ratio between the strengths of these two heat transfer mechanisms is determined by the so-called Richardson ($Ri = RaPr^2/Pe^2$) number, and mixed convection phenomena are particularly relevant for $0.1 < Ri < 10$.

In addition to numerous studies on mixed convection flow and heat transfer in fluid-only situations, mixed convective heat transfer in porous media is widely studied because of its practical relevance in for instance nuclear reactors [4], heat exchangers [5,6], solar collectors [7,8], geophysical systems [9] and electronic cooling [10]. Compared to fluid-only configurations, the presence of the porous medium significantly alters the flow and corresponding heat transfer [11–13]. An additional dimensionless parameter which now comes into play is the Darcy number, characterizing the permeability of the porous medium.

In literature, the great majority of experimental and numerical studies on pure natural [11,14,15] and forced [16–18] convection in porous media focus on the average flow and heat transfer features. A detailed collection of literature on mixed convective heat transfer in porous media

* Corresponding author.
E-mail address: M.Chakkingal@tudelft.nl (M. Chakkingal).
[1] M. Chakkingal and J. de Geus contributed equally to this manuscript.

https://doi.org/10.1016/j.icheatmasstransfer.2019.104457

Nomenclature

Greek symbols

α	Thermal diffusivity,$(k/\rho c_p)$, m^2/s
β	Coefficient of volume expansion of fluid, K^{-1}
λ	Thermal conductivity ratio of solid to fluid, k_s/k_f
ν	Kinematic viscosity of fluid, m^2/s
ϕ	Porosity
ρ	Density of fluid, kg/m^3

Abbreviations

ΔT	Temperature difference between the left and right walls K
$\mathbf{g}$	accel. due to gravity (acts along Z axis), m/s^2
$\mathbf{u}^*$	non-dimensionalized velocity
$\mathbf{u_w}$	moving wall velocity, m/s
$\mathbf{u}$	Pore-scale velocity, m/s
θ	Non-dimensional temperature, $\frac{T-T_c}{T_h-T_c}$
c_p	Specific heat capacity, J/kg.K
D	Darcy only
d	Diameter of sphere, m
$D+F$	Darcy and Forchheimer
Da	Darcy number, K/L^2
FC	Forced convection
K	Permeability
k	Thermal conductivity, W/m.K
k_m	Stagnant thermal conductivity of porous medium, k_m = 0.6 for water-hydrogel bead system, W/m.K
L	Height of cavity, m
MC	Mixed convection
NC	Natural convection
Nu_f	Nusselt number based on fluid properties, $-\frac{L}{\Delta T}\left(\frac{\partial T}{\partial y}\right)_{wall}$
Nu_{eff}	Relative strength of mixed convective heat transfer to that in natural and forced convection
p	Pressure, N/m^2
Pr_f	Prandtl Number based on fluid properties
Pr_m	Modified porous medium Prandtl Number, $Pr_f Da^{-0.5} C_f \times (k_f/k_m)$
Ra_f	Rayleigh Number based on fluid properties, $\frac{\mathbf{g}\beta_f \Delta T L^3}{\nu_f \alpha_f}$
Ra_m	Porous medium Rayleigh Number, $Ra_f Da(k_f/k_m)$
Re_m	Reynolds number porous medium, $\frac{u_w L}{\nu_f}\sqrt{Da}$
Ri	Richardson number, $\frac{Ra_f}{Pr_f Re_L^2}$
Ri_m	Modified Richardson number, $\frac{Ra_m}{Pr_m Re_m^2}$
T	Temperature, K
T_p	Combined temperature of the porous and fluid medium in Darcy simulation, K
T_{ref}	Reference temperature, $\frac{T_h+T_c}{2}$, K
VAM	volume averaged method
t_0	characteristic time scale, $\frac{L}{U_0}$, s
U_0	characteristic velocity scale, $\frac{Ra_f{}^{1/2}\alpha}{L}$, m/s
X, Y, Z	represents the rectangular coordinate system

Subscripts

a	Assisting
c	Cold
f	Fluid
h	Hot
n	Normal to the surface
o	Opposing
s	Solid

is reported in [19,20]. Most of the reported modelling studies were performed using a so-called Volume Averaging Method (VAM) approach to solve the large scale flow and temperature distributions in fine-grained porous media, applying Darcy and extended Darcy-type models for the flow and energy equations [21,22]. Such VAM-based numerical studies of so-called assisting mixed convection (i.e. mixed convection in which the induced natural convection flow is in the same direction as the imposed forced convection flow) in fine-grained porous media revealed a continuous enhancement of heat transfer with both increasing Rayleigh and Péclet numbers [23,24]. In contrast, for opposing forced convection, heat transfer initially decreases when Péclet number is increased at fixed Rayleigh number, followed by a gradual increase of heat transfer when Péclet is further increased [23].

Parametric studies of non-Darcy mixed convection in a vertical channel filled with a porous medium were performed in [25–27]. It was shown that the resulting heat transfer was enhanced when the Rayleigh and−/or Darcy numbers were increased. Effects of the conductivity ratio between the solid and the fluid, as well as different values of Darcy number were investigated in [28–34]. In most of the studies reported the contribution by forced convection is induced by moving the walls [35–37]. Though the flow close to the walls would differ from that in a cavity with a velocity inlet and an outlet (with zero flow velocity at the walls), a lid-driven cavity displays different phenomena like corner eddies, vortices, transition etc. in a comparatively simpler geometry [38], which makes it suitable to understand these phenomena observed in various real-life engineering applications like the ones listed above.

Modelling based on Darcy and extended Darcy-type of equations in combination with a form of the VAM does not suffice for situations characterized by relatively large pore scales. In particular, in numerous industrial and technological applications, such as gravel embankments [39], packed bed reactors [40], and the hearth of blast furnaces [41], the porous medium is coarse-grained, which means that the characteristic pore length scales are comparable to flow and thermal length scales [13]. For these situations, detailed insights into the local flow and temperature distributions are of crucial importance to understand local wall heat transfer phenomena, such as hot spots. Such insights, which can be obtained from modelling studies that fully resolve the geometrical structure of the coarse-grained porous medium, will reveal basic mechanisms for efficient flow and heat transfer control and potential optimizations. In our recent work on *pure natural* convection in coarse-grained porous media, we have attempted to explain the integral heat-transfer behaviour in terms of the local velocities and temperature distributions [12,13,42]. We observe the heat transfer to be dependent on the material of packing at low Rayleigh numbers, the effect of which decreases with the increase in Rayleigh number. However, what is still lacking in literature is insight in local, pore scale, flow and heat transfer mechanisms in *mixed* convection in coarse-grained porous media. In the current work, we study combined effect of forced convection induced by the motion of the cavity walls and natural convection due to the density difference induced by a horizontal temperature gradient in a porous media filled cavity. The current work aims at understanding the difference in heat transfer between coarse-grained simulations and Darcy/ extended-Darcy simulations in a generic mixed convective environment, like that in a lid-driven cavity and explain the difference based on local flow and temperature distribution.

2. Mathematical formulations and numerical methods

2.1. Physical problem

We analyze mixed convection in a differentially heated cubical

cavity with dimensions $L \times L \times L$, filled with water ($Pr_f = 5.4$) and packed with a coarse-grained porous medium (Fig. 1), at fluid Rayleigh numbers, $Ra_f = 10^6$ and 10^7. Spherical beads made of hydrogel (and thus having the same thermal properties as the fluid), are arranged in structured Body Centered Tetragonal (BCT) packing inside the cavity, to model a porous media filled cavity. The properties of the beads are chosen to be that of the fluid to avoid the complexity associated with the calculation of effective conductivity of the medium for Darcy and extended-Darcy simulations discussed below [43], which is out of the scope of current work. The ratio of the diameter of the beads, d to the length of the cavity, L is chosen to be 0.2. Finite dimensions of the cavity results in an average porosity of $\phi = 0.41$ (as opposed to $\phi = 0.302$ for an infinite BCT packing). The Darcy number, $Da = K/L^2 = \frac{\phi^3}{180(1-\phi)^2}\left(\frac{d}{L}\right)^2$ estimated using Kozeny–Carman equation is $Da \sim 4 \times 10^{-5}$ [14].

The coordinate system is chosen such that gravity, $\mathbf{g}$ acts in the direction of the negative Z axis. The left and right walls are at isothermal temperatures T_h and T_c ($T_h > T_c$) respectively. All the other walls of the cavity are adiabatic. No-slip boundary conditions are applied at all walls. The hot and cold walls are given equal and opposite velocities in the vertical direction to induce forced convection, which assists or opposes the natural convection, depending on the direction of the wall velocities:

1. **Assisting flow**: When the left hot wall moves in the upward direction ($\mathbf{u}_{wha}$) and the right cold wall moves in the downward direction ($\mathbf{u}_{wca}$) as shown by the solid vertical arrows, the forced convection assists the flow due to natural convection (Fig. 2a).
2. **Opposing flow**: When the left hot wall moves in the downward direction ($\mathbf{u}_{who}$) and the right cold wall moves in the upward direction ($\mathbf{u}_{wco}$) as shown by the solid vertical arrows, the forced convection opposes the flow due to natural convection (Fig. 2b).

The relative strength of natural convection over forced convection is expressed in terms of a modified Richardson number, Ri_m, based on a modified Rayleigh number, Ra_m, a modified Prandtl number Pr_m and a modified Reynolds number, Re_m, as introduced in [44] and defined in the Nomenclature of the present paper

$$Ri_m = \frac{Ra_m}{Pr_m Re_m^2} \tag{1}$$

A pre-multiplication factor, $C_f = 0.1$ is used in the calculation of Pr_m as discussed in [44]. For $Ri_m < < 1$ forced convection is dominant, whereas for $Ri_m > > 1$ the flow is dominated by natural convection.

In all studied cases, $\beta\Delta T < < 1$, and thus we ensure that the Boussinesq approximation [45] is valid. Thus assuming all the fluid properties, except the fluid density in the body forcing term of the Navier-Stokes (N-S) equations to be constant, the transient Navier-Stokes Eqs. (2), (3) and thermal energy transport equations Eqs. (4), (5) are solved numerically. The solid and fluid regions are thermally coupled at the interface using Dirichlet–Neumann Partitioning, to account for the conjugate heat transfer between the solid and the fluid region.

Fluid phase

$$\nabla \cdot \mathbf{u} = 0 \tag{2}$$

$$\frac{\partial \mathbf{u}}{\partial t} + \mathbf{u}\cdot\nabla\mathbf{u} = -\frac{1}{\rho_f}\nabla p + \nu\nabla^2\mathbf{u} + \mathbf{g}\beta(T_f - T_{ref}) \tag{3}$$

$$\frac{\partial T_f}{\partial t} + \mathbf{u}\cdot\nabla T_f = \alpha_f \nabla^2 T_f \tag{4}$$

Solid phase:

$$\frac{\partial T_s}{\partial t} = \alpha_s \nabla^2 T_s \tag{5}$$

At the coupled interface, we use Dirichlet and Neumann boundary conditions

$$T_f = T_s \tag{6}$$

to solve the fluid region.

$$k_f \frac{\partial T_f}{\partial n} = k_s \frac{\partial T_s}{\partial n} \tag{7}$$

to assure continuity of both the temperature and the heat flux at the fluid-solid interface.

The results from fully resolved coarse-grained media simulations are compared with Darcy-type VAM simulations (relative velocity resistance formulation). Here, the porous medium is modelled by taking the porosity, ϕ into account and by adding a momentum source term to the N-S equation [46]. A single thermal equation is used to model the energy transport.

$$\nabla \cdot \mathbf{u} = 0 \tag{8}$$

$$\frac{\partial \mathbf{u}}{\partial t} + \mathbf{u}\cdot\nabla\mathbf{u} = -\frac{1}{\rho_f}\nabla p + \nu\nabla^2\mathbf{u} + \mathbf{g}\beta(T_p - T_{ref}) + \frac{1}{\rho_f}\mathbf{S} \tag{9}$$

$$(\rho c_p)^* \frac{\partial T_p}{\partial t} + (\rho c_p)_f \phi \mathbf{u}\cdot\nabla T_p = k_m \nabla^2 T_p \tag{10}$$

where, $(\rho c_p)^* = \phi(\rho c_p)_f + (1-\phi)(\rho c_p)_s$. The source term, S is given by the Darcy-Forchheimer equation for homogeneous porous media:

$$\mathbf{S} = -\left(\mu D + \frac{1}{2}\rho_f \mid \phi\mathbf{u} \mid F\right)\phi\mathbf{u} \tag{11}$$

The first and second terms in S account for the viscous and inertial loss, respectively. In the present work, we use Ergun's equation [47] used for packed bed reactors giving:

$$D = \frac{150(1-\phi)^2}{d^2\phi^3} \tag{12}$$

$$F = \frac{3.5}{d}\frac{(1-\phi)}{\phi^3} \tag{13}$$

In addition to comparing results from fully resolved coarse grained media simulations to those obtained with the Darcy-Forchheimer model (Eqs. (8)–(13)), we also compare our results to Darcy model (Eqs. (8)–(12)) by setting the Forchheimer term (Eq. (13)) to zero.

2.2. Numerical method

The open-source, finite volume CFD solver OpenFOAM 2.4.0 [48] is used to carry out our simulations. Because of the complex nature of the

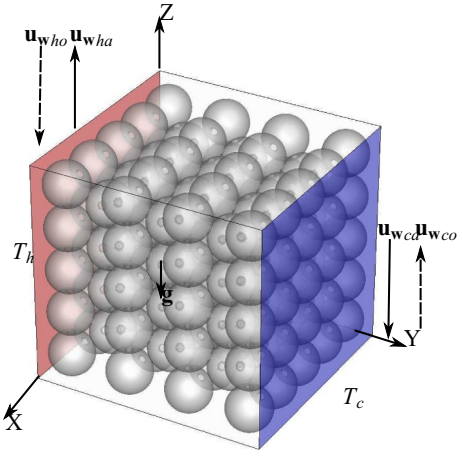

Fig. 1. Schematic representation of a hydrogel bead filled side heated cavity with the side walls at temperature T_c and T_h. The arrows show the direction of moving wall.

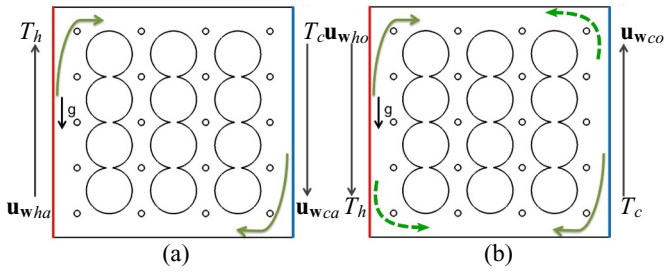

Fig. 2. 2D representation of (a) assisting (b) opposing mixed convection in a hydrogel bead filled side heated cavity with the side walls at temperature T_c and T_h. In (a) solid arrows show the net flow due to forced and natural convection; in (b) dashed arrows and solid arrows show the direction of flow induced by forced convection and natural convection respectively.

geometry in the fully resolved simulations, making it difficult to use structured grids, the sphere packed cubical cavities are meshed with body-conforming unstructured tetrahedral grids. With all the flows studied in this paper being either stationary or slowly oscillatory, the use of unstructured grids is reported in literature to be justified in terms of accuracy. Finn and Apte [49] report that OpenFOAM simulations of packed beds using unstructured meshes are comparable in accuracy to those on non-body-conforming cartesian grids, but with added computational costs. Similar studies on the accuracy of OpenFOAM simulations with unstructured grids are also reported in [50,51].

The above set of equations, Eqs. (2)–(5) are discretized and simulations are carried out using a modified version [13] of the standard conjugate heat transfer solver "chtMultiRegionFoam". The energy equation for the fluid region in the solver is modified as in "buoyantBoussinesqPimpleFoam" to account for the Boussinesq

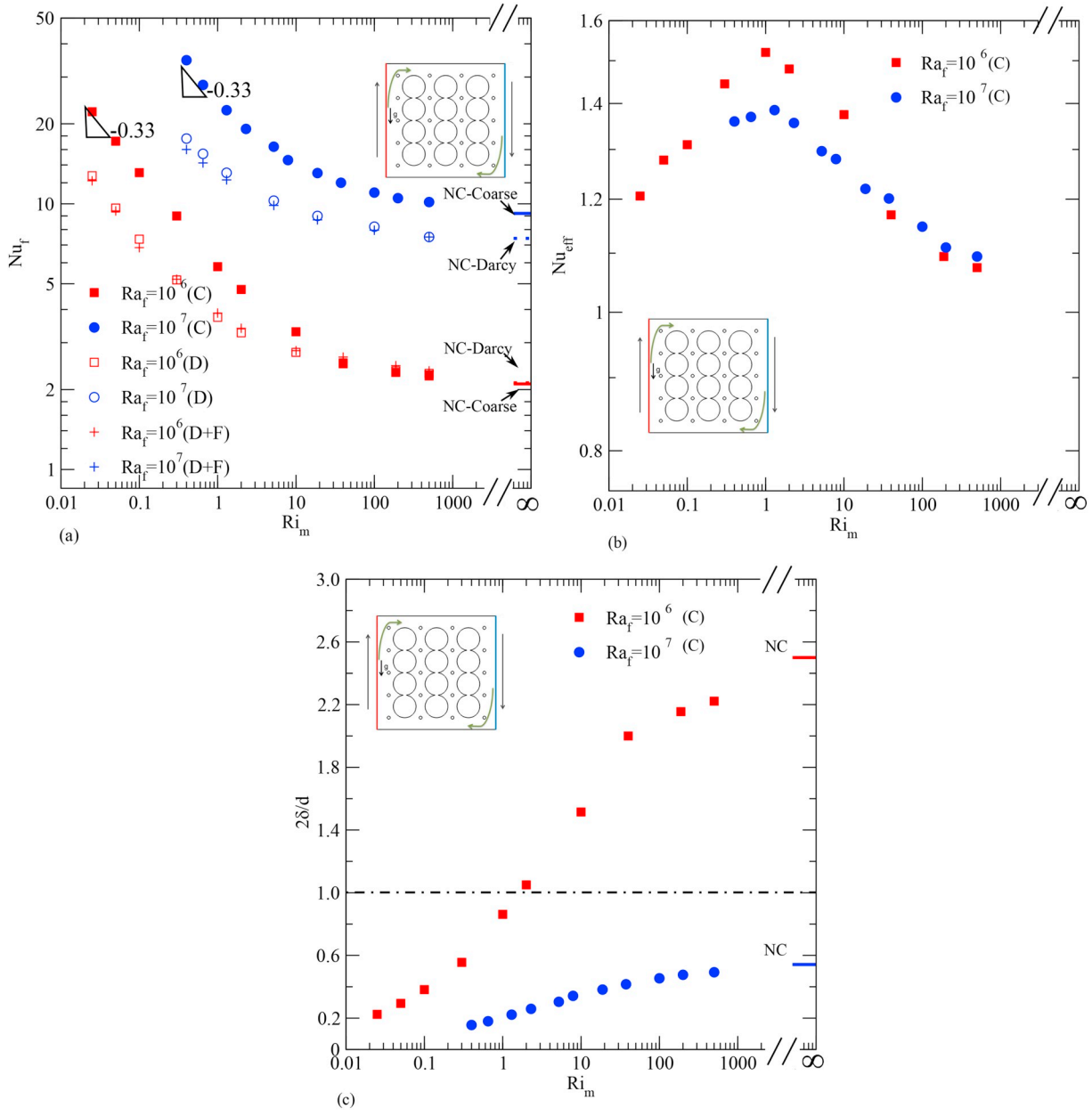

Fig. 3. Heat transfer and thermal boundary layer thickness variation in a coarse-grained porous media filled cavity with assisting mixed convection, at different Ra_f and Ri_m. Solid dash indicate the heat transfer in the hydrogel bead filled cavity with natural convection at $Ra_f = 10^6$(red), $Ra_f = 10^7$(blue) (a) total heat transfer (b) scaled effective heat transfer (c) boundary layer thickness in coarse-grained filled cavity. (For interpretation of the references to colour in this figure legend, the reader is referred to the web version of this article.)

approximation. We treat the temperature equation for the solid phase as a passive scalar equation. A detailed solver validation is reported in [13].

The Darcy and Darcy-Forchheimer simulations Eqs. (8)–(13) are solved by adding a porous zone to the "buoyantBoussinesqPimpleFoam" as discussed in [52].

In contrast to the fully resolved simulations, the Darcy simulations are carried out using a relatively coarse mesh consisting of hexahedral grid cells. The numerical schemes (available in OpenFOAM [48]) used to solve our equations are listed below:

1. Time stepping-backward scheme (2^{nd} order backward differencing scheme).
2. Convective and diffusive terms (Eqs. (3)–(10))-limitedLinear (2^{nd} order central differencing scheme).

The pressure-velocity-coupling at each time step is handled by the iterative PISO algorithm [53]. We solve the energy transport equation (Eq. (4)) using the divergence-free velocity obtained in each time step.

For the fully resolved simulations, a grid independence study is carried out using three different unstructured tetrahedral grids with 1.2×10^6, 5.1×10^6 and 1.12×10^7 grid cells, respectively. In all the simulations reported, 9 probes were inserted at random locations in the pore-space to monitor the time dependence of the flow and temperature. We place 3 probes each close to the isothermal walls at different heights with one at the central plane and the other two close to the front and back walls, while the remaining 3 probes are placed at the central plane with one in the pore-space close to the center of the cavity and the other 2 close to the top and bottom walls. In all cases, the flow and temperature was steady or slowly oscillating and in the laminar regime. Thus, we choose the overall Nusselt number to be the criterion to check the grid independence. At $Ra_f = 10^7$ and $Ri_m = 0.4$ the deviation in overall Nusselt number obtained between the 5.1×10^6 and

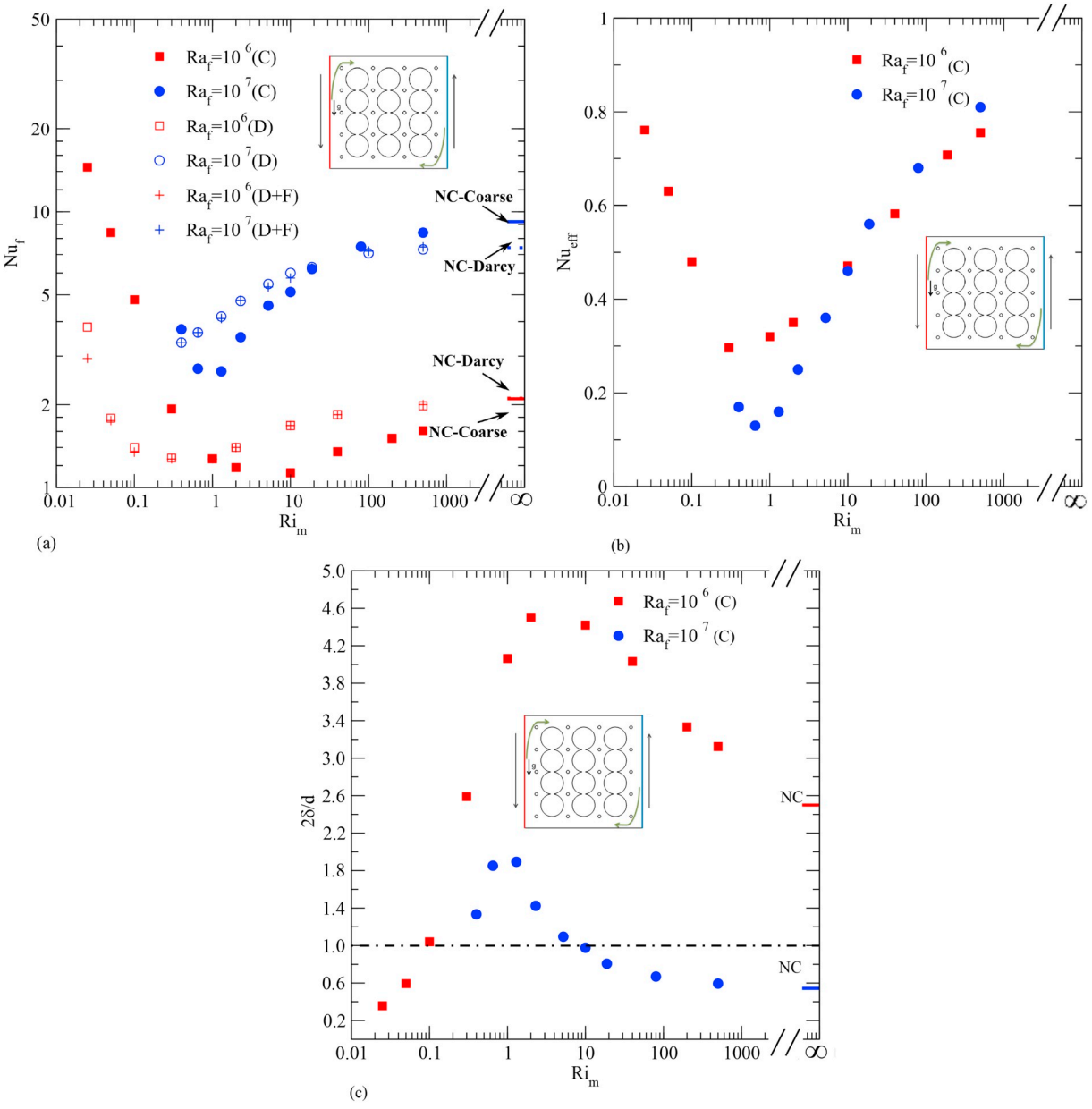

Fig. 4. Heat transfer and thermal boundary layer thickness variation in a coarse-grained porous media filled cavity with opposing mixed convection, at different Ra_f and Ri_m. Solid dash indicate the heat transfer in the hydrogel bead filled cavity with natural convection at $Ra_f = 10^6$(red), $Ra_f = 10^7$(blue) (a) total heat transfer (b) scaled effective heat transfer (c) boundary layer thickness in coarse-grained filled cavity. (For interpretation of the references to colour in this figure legend, the reader is referred to the web version of this article.)

1.12×10^7 grids is less than 3%. Consequently, the base grid cells for the presented simulations is set as 5.1×10^6 grid cells. This mesh is obtained by using a roughly uniform grid size $h \approx d/16 \approx L/80$ in the solid phase and in the core of the cavity. The same mesh size is used at the interfaces between the solid and fluid regions. Near the hot and cold walls the grid size is gradually refined to $h_{BL} \approx d/32 \approx L/160$.

A grid independence study for Darcy simulations is carried using 32^3, $64^3$and 128^3 hexahedral grid cells with an expansion factor of 1.2 close to the hot and cold walls. At $Ra_f = 10^7$ and $Ri_m = 0.4$, the deviation in overall Nusselt number obtained between the 64^3 and 128^3 hexahedral grid cells is less than 2%. Thus 128^3 hexahedral grid cells are used for our Darcy simulations.

An adaptive time stepping, with CFL number $=0.33$, is used in all the simulations reported. The time steps are observed to be constant throughout a simulation at fixed Ra_f, once the flow attains a (quasi) steady state.

3. Results and discussion

We study the combined effect of natural convection and forced convection in a cavity filled with a coarse-grained porous media, and compare results of fully resolved simulations to those of Darcy and Darcy-Forchheimer based volume averaged simulations. The temperature and velocities which are discussed below, are expressed in the non-dimensional form, such that the non-dimensional temperature, θ:

$$\theta = \frac{T - T_c}{T_h - T_c}$$

and non-dimensional velocity, $\mathbf{u}^*$:

$$\mathbf{u}^* = \frac{\mathbf{u}}{U_0}$$

where, $U_0 = \frac{Ra_f^{1/2\alpha}}{L}$ is the natural convection characteristic velocity scale defined as [54].

3.1. Analysis: Heat transfer at the isothermal walls

To understand the influence of the direction of the wall motion on the mixed convective heat transfer in a bead-filled cavity, we analyze the time and wall- averaged Nusselt number, Nu_f, as well as the scaled effective heat transfer (discussed below) in both assisting (Fig. 3) and opposing (Fig. 4) mixed convection, for $Ra_f = 10^6$ and 10^7 and $0.025 \leq Ri_m \leq 500$. The heat transfer results from the coarse-grained porous media simulations are compared with the results from Darcy simulations.

In assisting mixed convection (Fig. 3(a)), Nusselt numbers at $Ri_m > > 1$ approach that for pure natural convection alone (indicated as $Ri_m \to \infty$), as expected. At fixed Ra_f, heat transfer increases with decreasing Ri_m, i.e. increasing forced convection. For $Ri_m < < 1$, heat transfer is dominated by forced convection and indeed Nu_f scales as $Nu_f \sim {Ri_m}^{-0.33} \sim {Re_m}^{0.66}$, in agreement with what was found for forced convection heat transfer in a lid driven cavity [20,55]. Thus, heat transfer is dominated by natural convection at $Ri_m > > 1$, whereas it increases with decreasing Ri_m due to the combined contribution of natural convection and forced convection, and approaches that of pure forced convection for $Ri_m < < 1$. At $Ra_f = 10^6$, in the simulations at $Ri_m > 10$, the heat transfer in a coarse-grained porous media filled cavity is lower than that with Darcy assumption. The heat transfer due to natural convection alone exhibits the same behavior at $Ra_f = 10^6$. At $Ri_m < 10$, the heat transfer in coarse-grained simulations becomes higher than that in Darcy simulations. Unlike $Ra_f = 10^6$, at $Ra_f = 10^7$ and at all Ri_m, the heat transfer due to natural and assisting mixed convective flow in a coarse-grained porous media filled cavity is higher than that with Darcy assumption.

To quantify the range of Ri_m where natural convection and forced convection are of comparable strength, we define the effective heat transfer, Nu_{eff} as:

$$Nu_{eff} = \frac{Nu_{MC}}{Nu_{FC} + Nu_{NC} - 1} \tag{14}$$

with Nu_{MC} the observed mixed convection Nusselt number, Nu_{FC} the Nusselt number for forced convection only, and, Nu_{NC} the Nusselt number for natural convection only. Nu_{eff} quantifies the total heat transfer in mixed convection to the combined effect in natural convection alone and forced convection alone. We subtract 1 from the denominator to ensure that the effect of conduction is taken into account only once.

In assisting mixed convection Fig. 3(b), at both studied values of Ra_f, the effective heat transfer reaches a maximum at $Ri_m \approx 1$, i.e. when both natural and forced convection contribute equally to the heat transfer process. For $Ri_m < < 1$ and $Ri_m > > 1$, heat transfer is dominated by forced convection and natural convection respectively, resulting in Nu_{eff} approaching 1.

Comparing the fully resolved simulations (indicated by (C) in Fig. 3(a)), to those using Darcy-based and Darcy-Forchheimer based VAM models (indicated by (D) and (D + F) respectively), we observe that at $Ra_f = 10^6$ the heat transfer for natural convection dominated flows (i.e. large Ri_m, including pure natural convection at $Ri_m \to \infty$) in a coarse-grained porous medium filled cavity is lower than that obtained with the Darcy assumption, whereas at low Ri_m the heat transfer in coarse-grained simulations becomes higher than that in Darcy simulations. The cross-over is observed at $Ri_m \approx 10$. At $Ra_f = 10^7$ such a cross-over is not observed, and the heat transfer in a coarse-grained porous medium filled cavity is higher than that with the Darcy assumption at all Ri_m.

To understand this difference in behaviour at different Ra_f, we look at the relative thickness of the thermal boundary layers δ [11] compared to the radius $d/2$ of the beads:

$$\frac{2\delta}{d} = \frac{L/d}{Nu_f} \tag{15}$$

From Fig. 3(c) it is observed that at $Ra_f = 10^6$ the Darcy and Darcy-Forchheimer simulations under predict heat transfer when the thermal boundary layer thickness at the isothermal walls is significantly smaller than the radius of the beads. With the thinning of thermal boundary layer at higher $Ra_f = 10^7$, $2\delta/d$ is always less than 1, and Darcy simulations always under predict heat transfer.

We now move from assisting to opposing mixed convection (Fig. 4). As in assisting mixed convection, opposing mixed convection Nusselt numbers (see Fig. 4(a)) approach those in pure natural convection at high Ri_m, as expected. In deviation from assisting mixed convection, Nusselt decreases with decreasing Ri_m, i.e. increasing forced convection, and attains a minimum at $1 \leq Ri_m \leq 10$. With a further decrease in Ri_m, a change in the trend occurs and the Nusselt number increases, as heat transfer is now dominated by forced convection. In opposing mixed convection, the effective heat transfer (Fig. 4(b)), calculated as in Eq. (14), reaches a minimum at $Ri_m \approx 1$, representing the region where natural and forced convection are of equal strength and opposite to each other.

Comparing the fully resolved simulations (indicated by (C) in Fig. 4(a)), to those using Darcy-type VAM models (indicated by (D) and (D + F)), we observe that at $Ra_f = 10^6$ the heat transfer for high Ri_m natural convection dominated flows in a coarse-grained porous medium is lower than that obtained with the Darcy and Darcy-Forchheimer assumptions, whereas for low Ri_m forced convection dominated flows it becomes higher than that in Darcy-type simulations. At $Ra_f = 10^7$ the heat transfer in a coarse-grained porous medium filled cavity is lower than that with the Darcy and Darcy-Forchheimer assumptions for intermediate values of Ri_m, and approaches that of a Darcy-type medium for high Ri_m. This can again be understood by comparing the relative thickness of the thermal boundary layers to the radius of the beads. From Fig. 4(c) it is observed that at $Ra_f = 10^6$, the Darcy and Darcy-

Forchheimer simulations over-predict the heat transfer when the thermal boundary layer thickness is significantly larger than the bead size and under-predict it when the boundary layer thickness is significantly smaller. At $Ra_f = 10^7$, the thermal boundary layer thickness is larger than the bead size for all simulated $0.4 < Ri_m < 10$, in agreement with the range of Ri_m for which the coarse grained medium has a lower heat transfer than the Darcy-type medium.

To understand how the local heat transfer varies with the direction of the forced convection (i.e. of the moving wall), we compare the local instantaneous Nusselt number at the hot wall at $Ra_f = 10^7$ (Fig. 5). Compared to pure natural convection (Fig. 5(N1)), in assisting mixed convection (Fig. 5(A1,A2)) the overall heat transfer is increased and the regions of higher heat transfer extend further up along the hot wall.

On the other hand, in opposing mixed convection (Fig. 5(O1,O2)), the overall heat transfer is lower than that in natural convection, and with decreasing Ri_m, the regions where maximum heat transfer occurs shift to the top of the hot wall. This shows the change in the mode of heat transfer from natural convection to forced convection. The anti-clockwise motion of the fluid induced by the moving isothermal walls results in the change in the region of maximum heat transfer from the bottom to the top.

A comparison of heat transfer at the wall in coarse-grained porous media with Darcy simulations is reported in Fig. 6. As observed with coarse-grained media simulations, the simulations with Darcy assumption also show an increased overall heat transfer in assisting mixed convection and a change in the location of maximum heat transfer in

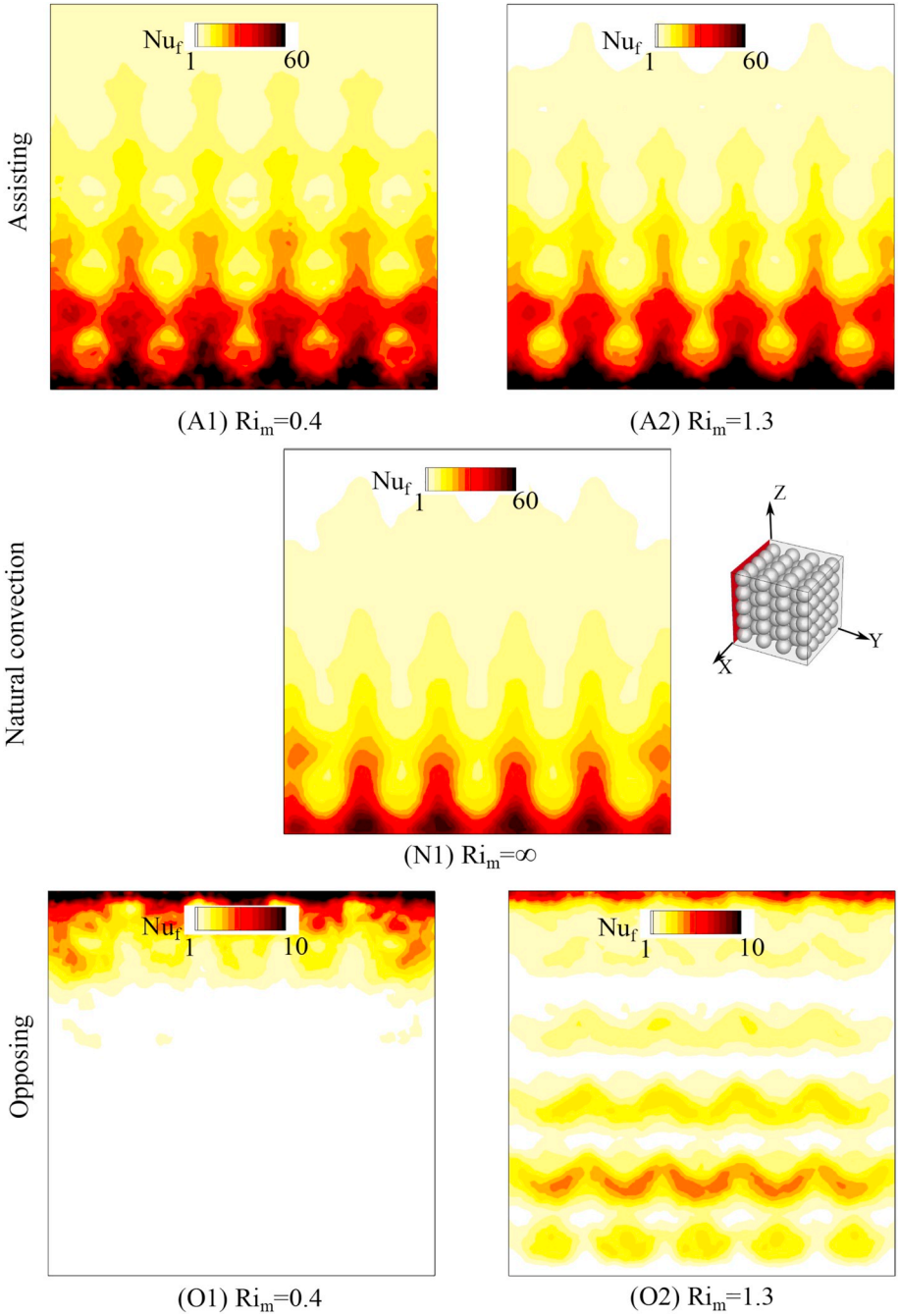

Fig. 5. Instantaneous Nusselt number Nu_f distributions at the hot wall in a cavity packed with hydrogel beads, at $Ra_f = 10^7$, at different Ri_m in assisting mixed convection (top row), natural convection (center) and opposing mixed convection (bottom row). The Nu_f distributions reported are at $t/t_0 = 30$, after a quasi steady-state has been reached.

opposing mixed convection. The heat transfer is observed to be uniform along the horizontal direction in Darcy simulations Fig. 6(A1,O1,N1), unlike the coarse-grained media simulations where the maximum heat transfer is limited to the pore-space Fig. 6(A2,N2,O2).

3.2. Spatial temperature and flow features at different Ri_m

To understand the spatial variations in heat transfer we analyze the local temperature and velocity fields from both fully resolved and Darcy

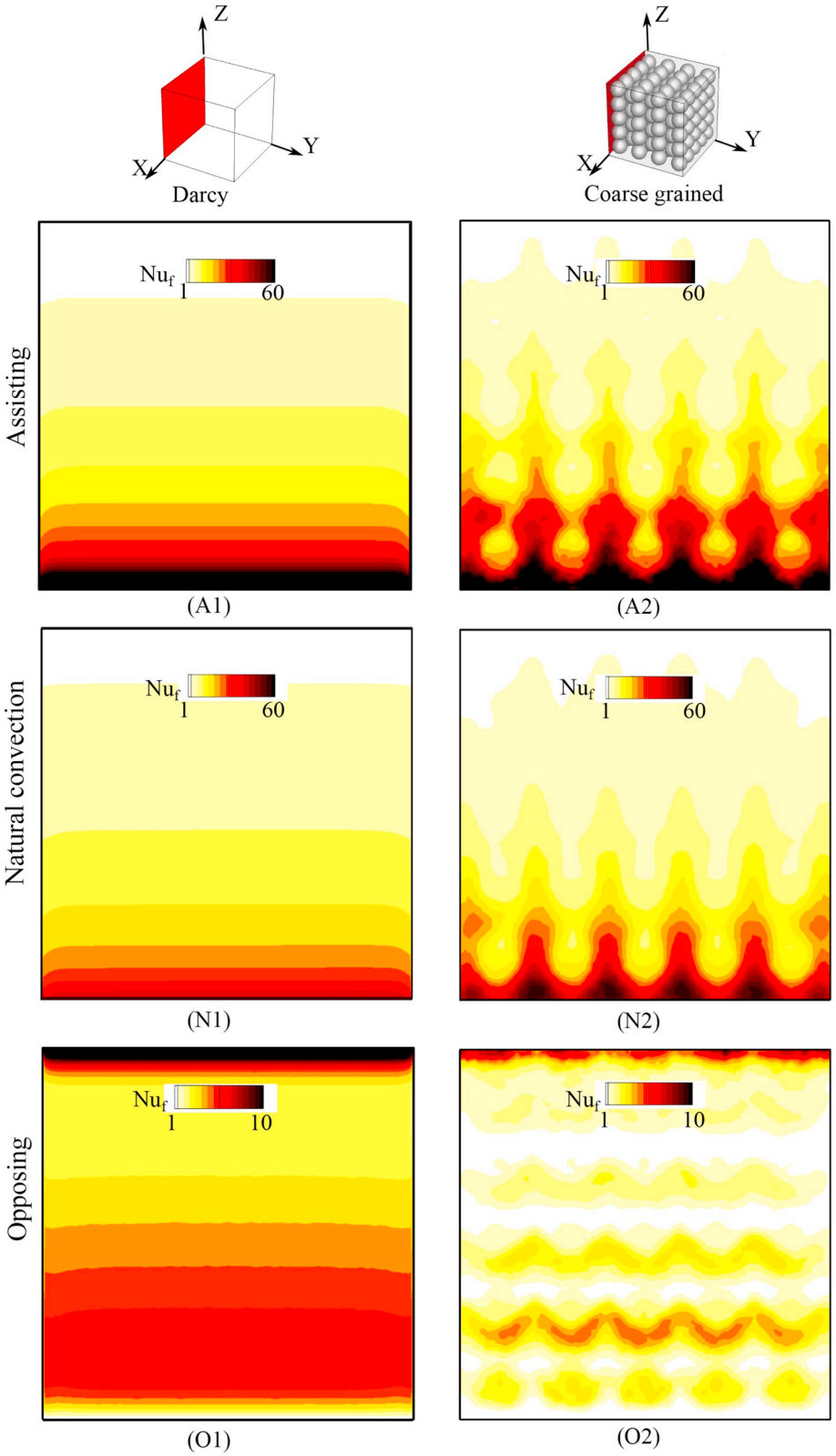

Fig. 6. Instantaneous Nusselt number Nu_f distributions at the hot wall at $Ra_f = 10^7$, $Ri_m = 1.3$ in assisting mixed convection (top row), natural convection (center) and opposing mixed convection (bottom row), with Darcy **(D)** assumption (left column) and coarse-grained **(C)** porous media filled cavity (right column). The Nu_f distributions reported are at $t/t_0 = 30$, after a quasi steady-state has been reached.

simulations. The nature of the flow structures at $Ra_f = 10^7$ is visible in Fig. 7, showing instantaneous $u_y - u_z$ velocity vectors in a characteristic vertical plane at $X/L = 0.79$. The flow field has reached a quasi steady-state, not changing over a period of $30t_0$, and the velocity field is interpolated on a 32–32 uniform grid for visualization purposes.

In pure natural convection (Fig. 7(N1,N2)), the temperature distribution and flow in coarse-grained and Darcy simulations are quite similar, but the flow velocities along the isothermal walls are a bit higher in the free pore spaces of the coarse-grained porous medium, because of the locally higher porosity and permeability. More importantly, and for similar reasons, higher velocities are observed in the free pore spaces along the horizontal adiabatic walls, causing cold fluid to impinge on the lower part of the hot wall, and hot fluid to impinge on the top part of the cold wall. Together this explains the slightly higher average Nusselt number observed for the coarse grained medium, as compared to the Darcy medium, shown in Fig. 3(a), as well as the increased local Nusselt number of the lower part of the hot wall, shown in Fig. 6(N2).

In assisting mixed convection (Fig. 7(A1,A2)), the velocities close to the isothermal walls increase compared to pure natural convection, leading to thinner thermal boundary layers. In the coarse grained medium, hot fluid impinges on the upper part of the cold wall with

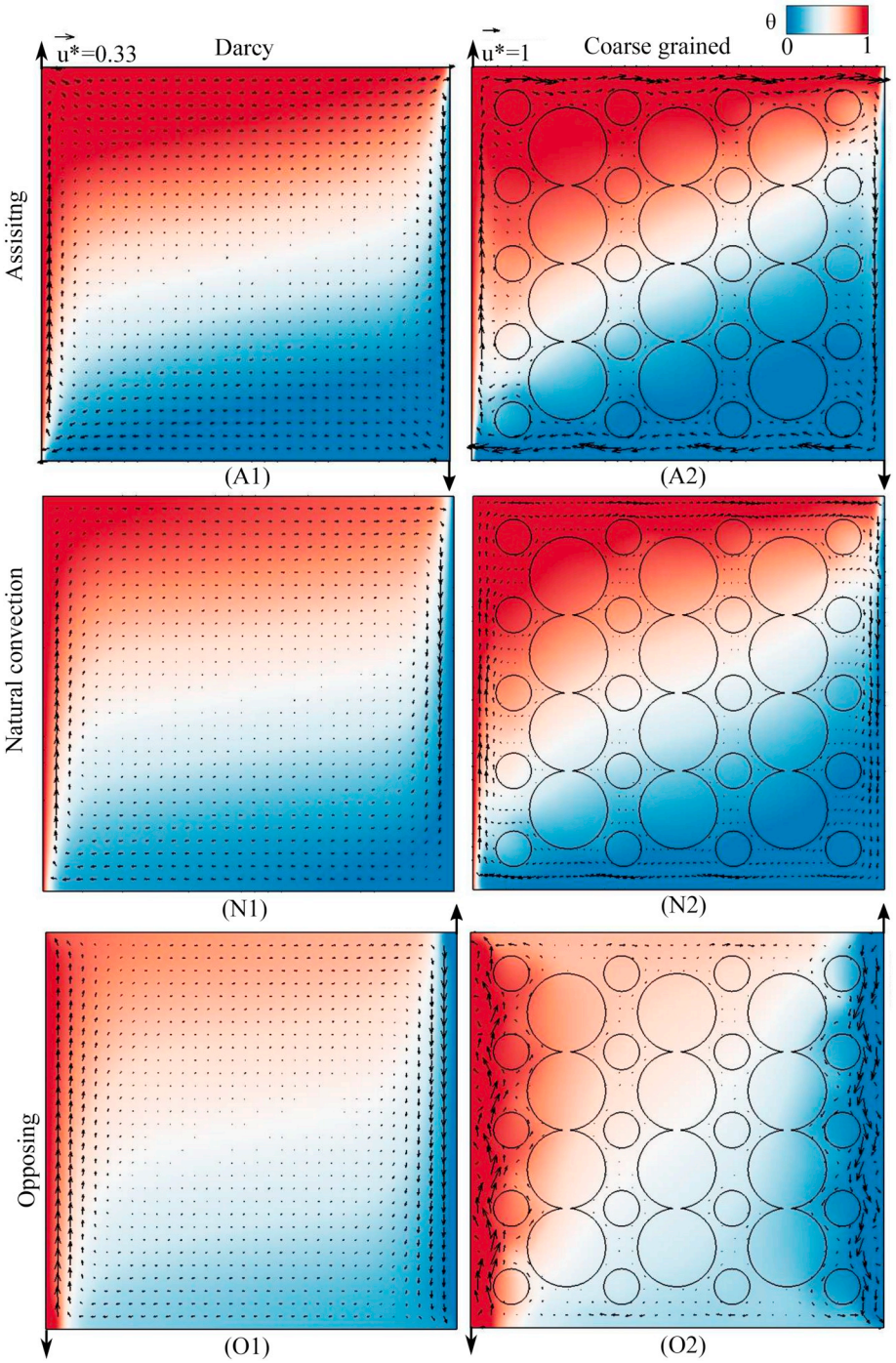

Fig. 7. Instantaneous velocity vectors and temperatures in a characteristic vertical plane, $X/L = 0.79$ at $Ra_f = 10^7$, $Ri_m = 1.3$ in assisting mixed convection (top row), natural convection (center) and opposing mixed convection (bottom row) with Darcy **(D)** assumption (left column) and coarse-grained **(C)** porous media filled cavity (right column). The instantaneous data reported is at $t/t_0 = 30$, after a quasi steady-state has been reached.

increased velocity, as does cold fluid on the lower part of the hot wall, explaining the 30% higher average Nusselt number for the coarse grained medium, shown in Fig. 3(a), and the increased local Nusselt number of the lower part of the hot wall, shown in Fig. 6(A2).

When the forced convection induced by the moving vertical walls is in the opposite direction w.r.t that in natural convection Fig. 7(O1,O2), we observe a change in the direction of flow close to the walls. The fluid close to the walls moves in the direction of the moving wall with the convective flow induced by natural convection in the opposite direction. The opposing nature of the flow results in thickening of the thermal boundary layer in both Darcy and coarse-grained media cavities.

In opposing mixed convection (Fig. 7(O1,O2)) we observe a flow direction reversal within the thermal boundary layers, resulting in two circulation zones extending from the bottom to the top of the cavity, close to the isothermal walls. Very close to the walls, the fluid moves in the direction of the moving wall, whereas a bit further away from the wall the flow is in the opposite direction due to buoyancy. This flow recirculation results in thickening of the thermal boundary layers and reduced average heat transfer (Fig. 3(a)), in both Darcy and coarse-grained medium. However, in the coarse-grained porous medium (Fig. 7(O2)), the opposing nature of forced and natural convection results in a local rotational flow in the pore-spaces close to the vertical walls. Due to increased mixing this leads to thick thermal boundary layers of uniform thickness, unlike the developing boundary layers in natural and assisting mixed convection (Fig. 7(N2,A2)), explaining the 40% lower average Nusselt number for the coarse grained medium, as shown in Fig. 3(a), and the decreased and more uniform local Nusselt number on the hot wall, as shown in Fig. 6(A2), both compared to the Darcy medium.

3.3. Local temperature and flow features at different Ri_m

From the above discussion it is clear that important differences in overall and local heat transfer between coarse-grained and Darcy-type simulations are due to differences in the local flow and temperatures. In the following sections we take a closer look at the local velocities and temperatures in the coarse-grained medium.

Fig. 8 shows the non-dimensional vertical velocity, u_z^* along the horizontal line at $Z/L = 0.5$ and $X/L = 0.4$, at $Ra_f = 10^7$ for different Ri_m. In assisting mixed convection (Fig. 8(a)), a transition from a natural convection boundary layer with a velocity extremum away from the wall, to a forced convection boundary layer with a velocity extremum at the wall, is observed for decreasing Ri_m (corresponding to an increasing Re_m). In opposing mixed convection (Fig. 8(b)), on the other hand, the local circulating flow induced by the opposing effects of wall motion and natural convection as discussed in Fig. 7(O1,O2), results in secondary extrema in the vertical velocities close to the first layer of hydrogel beads near the vertical walls.

Fig. 9 shows the local non-dimensional temperature, θ, both in the fluid and the hydrogel beads, along the horizontal line at $Z/L = 0.5$ and $X/L = 0.4$, at $Ra_f = 10^7$ for different Ri_m. In assisting mixed convection (Fig. 9 (a)), the temperature distribution exhibits clear and relatively thin thermal boundary layers for all $Ri_m \geq 0.4$, indicating the dominance of (either forced or natural) convective heat transfer. With increased contribution of forced convection (i.e. decreased Ri_m), the boundary layers get thinner and the local extrema close to isothermal walls become more prominent. In opposing mixed convection (Fig. 9(b)), on the other hand, the dominant mode of heat transfer switches from natural convection at high Ri_m to forced convection at low Ri_m via a "conduction only" mode at $Ri_m \sim 1$.

4. Summary and conclusion

We performed numerical simulations of assisting and opposing mixed convection in a side-heated, side-cooled lid driven cavity, packed with relatively large hydrogel beads, over a range of Richardson numbers, at fluid Rayleigh numbers 10^6 and 10^7. We focused on explaining overall heat transfer from local flow and temperature variations. The results are compared with Darcy and Darcy-Forchheimer simulations to understand the influence of the coarse-grained nature of the medium on the heat transfer. As in fluids-only mixed convection, in assisting mixed convection for a given Rayleigh number we find a maximum scaled effective heat transfer (and in opposing mixed convection we similarly find a scaled minimum effective heat transfer) at a Richardson number of approximately one, when the Richardson number is modified with the Darcy number Da and the Forchheimer coefficient $C_f = 0.1$ as $Ri_m = Ri \times Da^{0.5}/C_f$.

In assisting mixed convection we found a maximum heat transfer increase of $40 - 50\%$ for Rayleigh numbers between 10^6 and 10^7, compared to the summated heat transfer effects of natural and forced convection alone. In opposing mixed convection we found a maximum heat transfer decrease by a factor 3–10, for Rayleigh numbers between 10^6 and 10^7, compared to the summated heat transfer effects of natural and forced convection alone. We found that the ratio between the thermal boundary layer thickness at the isothermal walls and the average pore and sphere size plays an important role in the heat transfer mechanism and in the effect that the grain size has on the heat transfer. When this ratio is relatively large (i.e. at large solid object

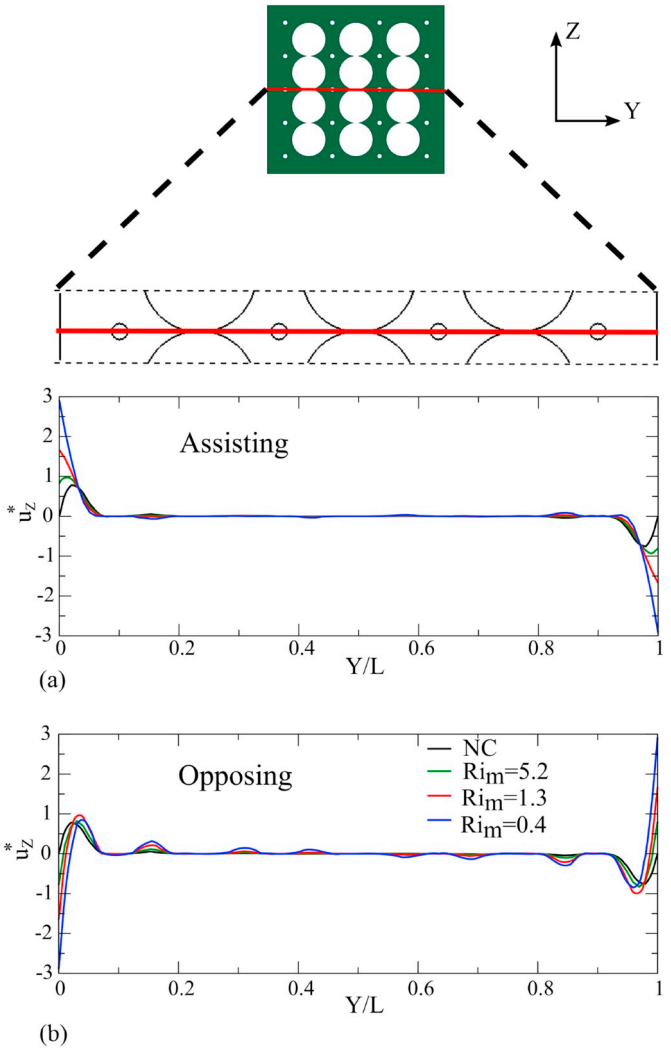

Fig. 8. Non-dimensional vertical velocity, u_z^* along the line at $Z/L = 0.5$ in the plane $X/L = 0.4$, at $Ra_f = 10^7$ in (a) assisting mixed convection (b) opposing mixed convection at different Ri_m. The instantaneous vertical velocity reported is at $t/t_0 = 30$, after a quasi steady-state has been reached.

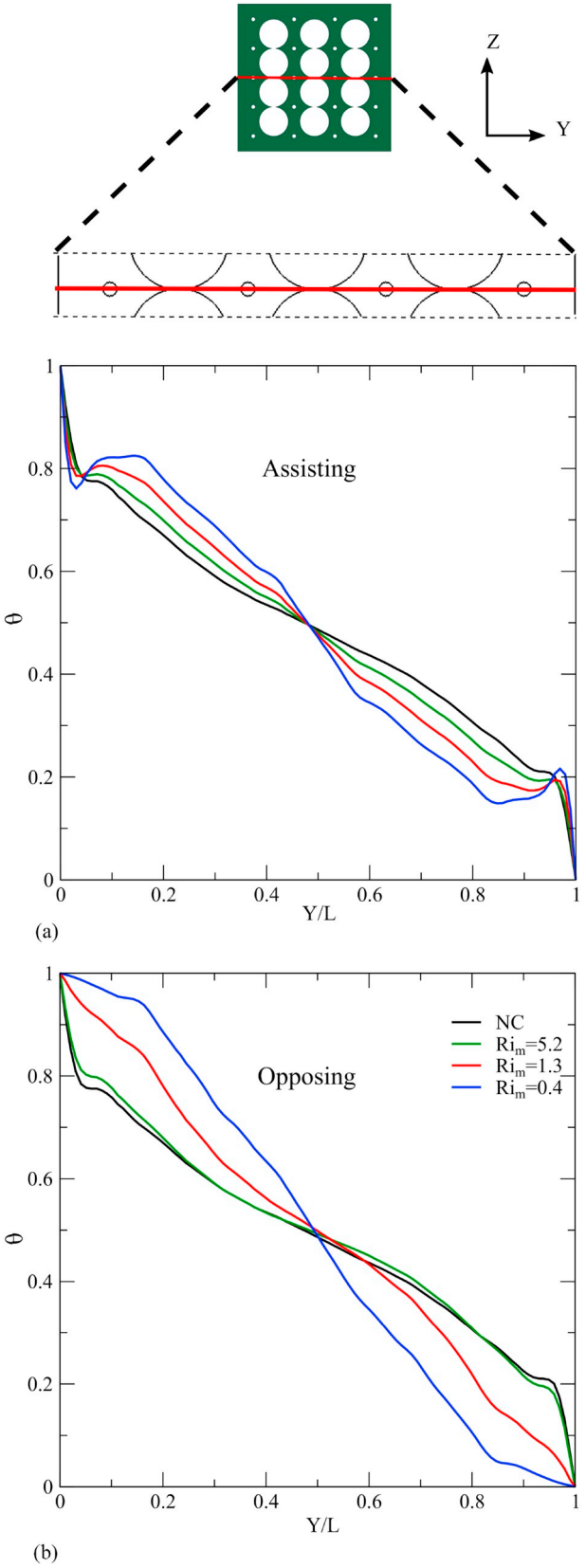

Fig. 9. Non-dimensional temperature along the line at $Z/L = 0.5$ in the plane $X/L = 0.4$, at $Ra_f = 10^7$ in (a) assisting mixed convection (b) opposing mixed convection at different Ri_m. The instantaneous temperature reported is at $t/t_0 = 30$, after a quasi steady-state has been reached.

dimensions and/or high Rayleigh numbers), the thermal boundary layer is locally disturbed by the solid objects and these objects cause local velocities and flow recirculation perpendicular to the walls. As a result, for a coarse grained medium we not only find strong local variations in heat transfer, but also significant differences in the wall-average heat transfer. Our ongoing experimental study on mixed convection in porous-media filled cavities with an inlet and outlet also hints at the influence of coarse-grained porous media on local and integral heat transfer. For such coarse grained media, either fully resolved simulations, or simulations applying more sophisticated VAM models than Darcy-type models, are needed to predict both local and average heat transfer. From our previous work on natural convection with similar packing, we find a strong influence of material properties on heat transfer at low Rayleigh numbers which decreases with the increase in Rayleigh number. It would also be interesting to investigate the influence of material properties on the flow and heat transfer in coarse-grained porous media filled cavities under mixed convection. As observed in the current work, we expect a transition from heat transfer dominated by natural convection to that by forced convection to occur in assisting and opposing cases, but at different Richardson numbers depending on the thermal properties of the porous media.

Declaration of Competing Interest

None.

Acknowledgments

This research was carried out under project number S41.5.14526a in the framework of the Partnership Program of the Materials innovation institute M2i (www.m2i.nl) and the Technology Foundation TTW (www.stw.nl), which is part of the Netherlands Organization for Scientific Research (www.nwo.nl). We would like to thank our industrial partner TATA Steel, The Netherlands, for continuous financial support and SURFsara for the support in using the Cartesius Computing Cluster (NWO File No.175507128).

References

[1] A. Raji, M. Hasnaoui, Mixed convection heat transfer in a rectangular cavity ventilated and heated from the side, Num. Heat Transf. Part A: Appl. 33 (5) (1998) 533–548, https://doi.org/10.1080/10407789808913953.
[2] H.F. Oztop, I. Dagtekin, Mixed convection in two-sided lid-driven differentially heated square cavity, Int. J. Heat Mass Transf. 47 (8–9) (2004) 1761–1769, https://doi.org/10.1016/j.ijheatmasstransfer.2003.10.016.
[3] A.K. Prasad, J.R. Koseff, Combined forced and natural convection heat transfer in a deep lid-driven cavity flow, Int. J. Heat Fluid Flow 17 (5) (1996) 460–467, https://doi.org/10.1016/0142-727x(96)00054-9.
[4] T.S. Ro, N.E. Todreas, Energy transfer mechanisms in LMR rod bundles under mixed convection conditions, Nucl. Eng. Des. 108 (3) (1988) 343–357, https://doi.org/10.1016/0029-5493(88)90223-3.
[5] J. Sillekens, C. Rindt, A.V. Steenhoven, Developing mixed convection in a coiled heat exchanger, Int. J. Heat Mass Transf. 41 (1) (1998) 61–72, https://doi.org/10.1016/s0017-9310(97)00111-7.
[6] N. Ghorbani, H. Taherian, M. Gorji, H. Mirgolbabaei, Experimental study of mixed convection heat transfer in vertical helically coiled tube heat exchangers, Exp. Thermal Fluid Sci. 34 (7) (2010) 900–905, https://doi.org/10.1016/j.expthermflusci.2010.02.004.
[7] Z. Li, Z. Huang, W. Tao, Three-dimensional numerical study on turbulent mixed convection in parabolic trough solar receiver tube, Energy Procedia 75 (2015) 462–466, https://doi.org/10.1016/j.egypro.2015.07.422.
[8] M.C. Moghadam, M. Edalatpour, J.P. Solano, Numerical study on conjugated laminar mixed convection of alumina/water nanofluid flow, heat transfer, and entropy generation within a tube-on-sheet flat plate solar collector, J. Solar Energy Eng. 139 (4) (2017) 041011, , https://doi.org/10.1115/1.4036854.
[9] A.J. Smith, Mixed convection and density-dependent seawater circulation in coastal aquifers, Water Resour. Res. 40 (8) (aug 2004), https://doi.org/10.1029/2003wr002977.
[10] F.P. Incropera, Convection heat transfer in electronic equipment cooling, J. Heat Transf. 110 (4b) (1988) 1097, https://doi.org/10.1115/1.3250613.
[11] D.J. Keene, R.J. Goldstein, Thermal convection in porous media at high rayleigh numbers, J. Heat Transf. 137 (2015) 1–4, https://doi.org/10.1115/1.4029087.
[12] I. Ataei-Dadavi, M. Chakkingal, S. Kenjereš, C.R. Kleijn, M.J. Tummers, Flow and heat transfer measurements in natural convection in coarse-grained porous media,

Int. J. Heat Mass Transf. 130 (2019) 575–584, https://doi.org/10.1016/j.ijheatmasstransfer.2018.10.118.
[13] M. Chakkingal, S. Kenjereš, I. Ataei-Dadavi, M. Tummers, C.R. Kleijn, Numerical analysis of natural convection with conjugate heat transfer in coarse-grained porous media, Int. J. Heat Fluid Flow 77 (2019) 48–60, https://doi.org/10.1016/j.ijheatfluidflow.2019.03.008.
[14] T. Jonsson, I. Catton, Prandtl number dependence of natural convection in porous media, J. Heat Transf. 109 (2) (1987) 371, https://doi.org/10.1115/1.3248090.
[15] C.R.B. Lister, An explanation for the multivalued heat transport found experimentally for convection in a porous medium, J. Fluid Mech. 214 (1990) 287–320, https://doi.org/10.1017/S0022112090000143.
[16] V. Calmidi, R. Mahajan, Forced convection in high porosity metal foams, J. Heat Transf. 122 (3) (2000) 557–565, https://doi.org/10.1115/1.1287793.
[17] D. Nield, A. Kuznetsov, M. Xiong, Thermally developing forced convection in a porous medium: parallel plate channel with walls at uniform temperature, with axial conduction and viscous dissipation effects, Int. J. Heat Mass Transf. 46 (4) (2003) 643–651, https://doi.org/10.1016/S0017-9310(02)00327-7.
[18] B. Buonomo, O. Manca, G. Lauriat, Forced convection in micro-channels filled with porous media in local thermal non-equilibrium conditions, Int. J. Therm. Sci. 77 (2014) 206–222, https://doi.org/10.1016/j.ijthermalsci.2013.11.003.
[19] D.B. Ingham, I. Pop, Transport Phenomena in Porous Media II, (2002), https://doi.org/10.1007/BF00615200.
[20] D.A. Nield, A. Bejan, Convection in Porous Media, Springer New York, 2013, https://doi.org/10.1007/978-1-4614-5541-7.
[21] J. Koh, R. Colony, Heat transfer of microstructure for integrated circuits, Int. Commun. Heat Mass Transf. 13 (1) (1986) 89–98, https://doi.org/10.1016/0735-1933(86)90075-8 https://doi.org/10.1016/0735-1933(86)90075-8.
[22] K.M. Khanafer, A.J. Chamkha, Mixed convection flow in a lid-driven enclosure filled with a fluid-saturated porous medium, Int. J. Heat Mass Transf. 42 (13) (1999) 2465–2481, https://doi.org/10.1016/s0017-9310(98)00227-0.
[23] F.-C. Lai, V. Prasad, F. Kulacki, Aiding and opposing mixed convection in a vertical porous layer with a finite wall heat source, Int. J. Heat Mass Transf. 31 (5) (1988) 1049–1061, https://doi.org/10.1016/0017-9310(88)90093-2.
[24] K. Muralidhar, Mixed convection flow in a saturated porous annulus, Int. J. Heat Mass Transf. 32 (5) (1989) 881–888, https://doi.org/10.1016/0017-9310(89)90237-8.
[25] A. Hadim, Numerical study of non-darcy mixed convection in a vertical porous channel, J. Thermophys. Heat Transf. 8 (2) (1994) 371–373, https://doi.org/10.2514/3.549.
[26] A. Hadim, G. Chen, Non-darcy mixed convection in a vertical porous channel with discrete heat sources at the walls, Int. Commun. Heat Mass Transf. 21 (3) (1994) 377–387, https://doi.org/10.1016/0735-1933(94)90006-X.
[27] Y. Chen, J. Chung, C. Wu, Y. Lue, Non-darcy mixed convection in a vertical channel filled with a porous medium, Int. J. Heat Mass Transf. 43 (13) (2000) 2421–2429, https://doi.org/10.1016/s0017-9310(99)00299-9.
[28] N.H. Saeid, Analysis of mixed convection in a vertical porous layer using non-equilibrium model, Int. J. Heat Mass Transf. 47 (26) (2004) 5619–5627, https://doi.org/10.1016/j.ijheatmasstransfer.2004.07.033.
[29] K.-C. Wong, N.H. Saeid, Numerical study of mixed convection on jet impingement cooling in a horizontal porous layer under local thermal non-equilibrium conditions, Int. J. Therm. Sci. 48 (5) (2009) 860–870, https://doi.org/10.1016/j.ijthermalsci.2008.06.004.
[30] G. Venugopal, C. Balaji, S. Venkateshan, Experimental study of mixed convection heat transfer in a vertical duct filled with metallic porous structures, Int. J. Therm. Sci. 49 (2) (2010) 340–348, https://doi.org/10.1016/j.ijthermalsci.2009.07.018.
[31] N.S. Ahmed, I.A. Badruddin, J. Kanesan, Z. Zainal, K.N. Ahamed, Study of mixed convection in an annular vertical cylinder filled with saturated porous medium, using thermal non-equilibrium model, Int. J. Heat Mass Transf. 54 (17–18) (2011) 3822–3825, https://doi.org/10.1016/j.ijheatmasstransfer.2011.05.001.
[32] M.K. Khandelwal, P. Bera, A thermal non-equilibrium perspective on mixed convection in a vertical channel, Int. J. Therm. Sci. 56 (2012) 23–34, https://doi.org/10.1016/j.ijthermalsci.2012.01.014.
[33] B. Buonomo, G. Cresci, O. Manca, P. Mesolella, S. Nardini, Transient mixed convection in a channel with an open cavity filled with porous media, J. Phys. Conf. Ser. 395 (1) (2012) 12149.
[34] H. Çelik, M. Mobedi, O. Manca, U. Ozkol, A pore scale analysis for determination of interfacial convective heat transfer coefficient for thin periodic porous media under mixed convection, Int. J. Num. Methods Heat Fluid Flow 27 (12) (2017) 2775–2798, https://doi.org/10.1108/hff-01-2017-0036.
[35] H.F. Oztop, Combined convection heat transfer in a porous lid-driven enclosure due to heater with finite length, Int. Commun. Heat Mass Transf. 33 (6) (2006) 772–779, https://doi.org/10.1016/j.icheatmasstransfer.2006.02.003.
[36] E. Vishnuvardhanarao, M.K. Das, Laminar mixed convection in a parallel two-sided lid-driven differentially heated square cavity filled with a fluid-saturated porous medium, Num. Heat Transf. Part A: Appl. 53 (1) (2007) 88–110, https://doi.org/10.1080/10407780701454006.
[37] E. Vishnuvardhanarao, M.K. Das, Mixed convection in a buoyancy-assisted two-sided lid-driven cavity filled with a porous medium, Int. J. Num. Methods Heat Fluid Flow 19 (3/4) (2009) 329–351, https://doi.org/10.1108/09615530910938317.
[38] P.N. Shankar, M.D. Deshpande, Fluid mechanics in the driven cavity, Annu. Rev. Fluid Mech. 32 (1) (2000) 93–136, https://doi.org/10.1146/annurev.fluid.32.1.93.
[39] D.J. Goering, P. Kumar, Winter-time convection in open-graded embankments, Cold Reg. Sci. Technol. 24 (1) (1996) 57–74, https://doi.org/10.1016/0165-232X(95)00011-Y.
[40] D.J. Gunn, Transfer of heat or mass to particles in fixed and fluidised beds, Int. J. Heat Mass Transf. 21 (4) (1978) 467–476, https://doi.org/10.1016/0017-9310(78)90080-7.
[41] S. Ueda, S. Natsui, H. Nogami, J.-I. Yagi, T. Ariyama, Recent progress and future perspective on mathematical modeling of blast furnace, ISIJ Int. 50 (7) (2010) 914–923, https://doi.org/10.2355/isijinternational.50.914.
[42] I. Ataei-Dadavi, N. Rounaghi, M. Chakkingal, S. Kenjeres, C.R. Kleijn, M.J. Tummers, An experimental study of flow and heat transfer in a differentially side heated cavity filled with coarse porous media, Int. J. Heat Mass Transf. 143 (2019) 118591, , https://doi.org/10.1016/j.ijheatmasstransfer.2019.118591.
[43] M. Kandula, On the effective thermal conductivity of porous packed beds with uniform spherical particles, J. Porous Media 14 (10) (2011).
[44] V. Kathare, J.H. Davidson, F.A. Kulacki, Natural convection in water-saturated metal foam, Int. J. Heat Mass Transf. 51 (15–16) (2008) 3794–3802, https://doi.org/10.1016/j.ijheatmasstransfer.2007.11.051.
[45] D.D. Gray, A. Giorgini, The validity of the boussinesq approximation for liquids and gases, Int. J. Heat Mass Transf. 19 (5) (1976) 545–551, https://doi.org/10.1016/0017-9310(76)90168-X.
[46] P. Nithiarasu, K. Seetharamu, T. Sundararajan, Natural convective heat transfer in a fluid saturated variable porosity medium, Int. J. Heat Mass Transf. 40 (16) (1997) 3955–3967, https://doi.org/10.1016/s0017-9310(97)00008-2.
[47] S. Ergun, A.A. Orning, Fluid flow through randomly packed columns and fluidized beds, Ind. Eng. Chem. 41 (6) (1949) 1179–1184, https://doi.org/10.1021/ie50474a011.
[48] H.G. Weller, G. Tabor, H. Jasak, C. Fureby, A tensorial approach to computational continuum mechanics using object-oriented techniques, Comput. Phys. 12 (6) (1998) 620–631, https://doi.org/10.1063/1.168744.
[49] J. Finn, S.V. Apte, Relative performance of body fitted and fictitious domain simulations of flow through fixed packed beds of spheres, Int. J. Multiphase Flow 56 (2013) 54–71, https://doi.org/10.1016/j.ijmultiphaseflow.2013.05.001.
[50] A. Zenklusen, S. Kenjereš, P.R. von Rohr, Vortex shedding in a highly porous structure, Chem. Eng. Sci. 106 (2014) 253–263, https://doi.org/10.1016/j.ces.2013.11.022.
[51] A. Zenklusen, S. Kenjereš, P.R. von Rohr, Mixing at high Schmidt number in a complex porous structure, Chem. Eng. Sci. 150 (2016) 74–84, https://doi.org/10.1016/j.ces.2016.04.057.
[52] H.E. Hafsteinsson, Porous media in OpenFOAM, CFD with Opensource Software, Tech. rep., Chalmers University of Technology, (2009).
[53] R. Issa, Solution of the implicitly discretised fluid flow equations by operator-splitting, J. Comput. Phys. 62 (1) (1986) 40–65, https://doi.org/10.1016/0021-9991(86)90099-9.
[54] J. Patterson, J. Imberger, Unsteady natural convection in a rectangular cavity, J. Fluid Mech. 100 (1) (1980) 65, https://doi.org/10.1017/S0022112080001012.
[55] N. Wakao, S. Kaguei, Heat and Mass Transfer in Packed Beds, (1982).